Pure Appl. Chem., Vol. 79, No. 6, pp. 1023–1039, 2007.
doi:10.1351/pac200779061023

Proton transfer across hydrogen bonds: From reaction path to Schrödinger's cat*

François Fillaux[1,‡], Alain Cousson[2], and Matthias J. Gutmann[3]

[1]LADIR-CNRS, UMR 7075, Université P. et M. Curie, 2 rue Henry Dunant, 94320 Thiais, France; [2]Laboratoire Léon Brillouin (CEA-CNRS), C.E. Saclay, 91191 Gif-sur-Yvette, Cedex, France; [3]ISIS Facility, Rutherford Appleton Laboratory, Chilton, Didcot, OX11 0QX, UK

Abstract: We review recent studies of the interconversion mechanism of OH···O hydrogen-bonded centrosymmetric dimers through proton transfer in the prototype crystals of potassium hydrogen carbonate ($KHCO_3$) and benzoic acid (C_6H_5COOH). The point at issue is whether the proton distributions at various temperatures arise from classical statistical mixtures of tautomers or quantum mechanical superposition states. A related issue is whether it is possible to probe a quantum superposition without inducing decoherence and classicality. We show that neutron diffraction can realize decoherence-free measurements for strictly defined scattering geometries and thus evidence macroscopic quantum correlations. We present a theoretical framework for decoherence-free macroscopically entangled states of the sublattice of protons. The neutron diffraction cross-section of protons is enhanced by a factor of ≈45, compared to regular Bragg diffraction, and quantum correlations are observed with remarkable contrast. At elevated temperatures, up to 300 K, quantum correlations are unaffected by proton transfer. The crystal is a coherent superposition of macroscopic tunnelling states, like Schrödinger's cat in a superposition of dead and alive states.

Keywords: hydrogen bonding; proton transfer; quantum tunnelling; tautomerism; neutron scattering; quantum entanglement.

INTRODUCTION

Proton transfer across hydrogen bonds is of fundamental importance to many physical, chemical, and biophysical processes [1–7]. There is a general agreement that dynamics can be modeled as light particles moving along local reaction coordinates coupled to the motion of heavy atoms. These dynamics are dominated by strong quantum effects with pronounced sensitivity to isotope substitution.

In the crystalline state, potassium hydrogen carbonate ($KHCO_3$) and benzoic acid (C_6H_5COOH) form centrosymmetric dimers linked by moderately strong hydrogen bonds, OH···O. At the temperature of liquid helium, neutron diffraction shows protons located, within experimental accuracy >99%, at the same crystallographic configuration (say **T1** in Fig. 1). As the temperature is increased, protons are progressively transferred to **T2** [8–10]. This thermally activated interconversion, or tautomerism, is monitored by proton dynamics.

*Paper based on a presentation at the 18th International Conference on Physical Organic Chemistry (ICPOC-18), 20–25 August 2006, Warsaw, Poland. Other presentations are published in this issue, pp. 955–1151.

‡Corresponding author: E-mail: fillaux@glvt-cnrs.fr

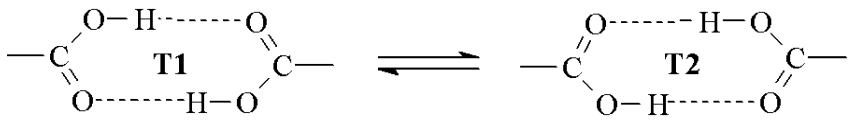

Fig. 1 Sketch of the tautomeric equilibrium of centrosymmetric hydrogen-bonded dimers.

Experimental studies utilizing NMR, quasi-elastic neutron scattering (QENS), and vibrational spectroscopy techniques converge to the conclusion that proton transfer occurs across an asymmetric double minimum potential [8,9,11–26]. However, rather different dynamical models have been proposed. Among them, one can distinguish two classes we shall term "reaction-path" and "Schrödinger's cat", respectively.

In the reaction-path model, interconversion is represented as a chemical equilibrium between uncorrelated tautomers (Fig. 1), leading to stochastic disorder at elevated temperatures [11,12,15,16,18,19,21–23,26]. In the semiclassical limit, the proton is treated as a dimensionless particle, and reorganization of the single-bond/double-bond structure during the transfer defines the reaction path over a multidimensional potential energy surface. The "phonon-assisted" interconversion is monitored by displacements of the heavy atoms coupled to the thermal bath. At low temperatures, the transfer rate is dominated by "phonon-assisted incoherent tunnelling". At elevated temperatures, there is a transition from the quantum to the classical regime when over-barrier proton jumps prevail.

This model accounts for solid-state NMR and QENS measurements. However, the stochastic disorder of protons and dimers is at variance with recent neutron diffraction works. The long-range space-coherence of proton positions should be destroyed and lead to an apparent decrease of the total amount of protons (or probability density), compared to the known stoichiometry [27,28]. In fact, this is not observed [8–10]. The spatial coherence of protons survives at elevated temperatures, and proton transfer must be thought of as a large-scale coherent process.

In the alternative "coherent tunnelling" model, interconversion arises from the quantum superposition in thermal equilibrium of states, $a(T)|\mathbf{I}\rangle + b(t)|\mathbf{II}\rangle$, with $a^2 + b^2 = 1$ (Fig. 2), analogous to Schrödinger's cat in a superposition of "dead–alive" states. The proton-transfer dynamics is adiabatically separated from the lattice of heavy atoms, and the superposition yields harmonic oscillations of protons between the two configurations, through quantum beats. This model is straightforward in the gas phase since the two forms are indistinguishable [29]. In the crystalline state, the quantum superposition is, in principle, permitted by quantum mechanics, but the environment-induced decoherence is supposed to lead extremely rapidly to a statistical mixture of the two configurations [30] for which quantum interferences are no longer possible.

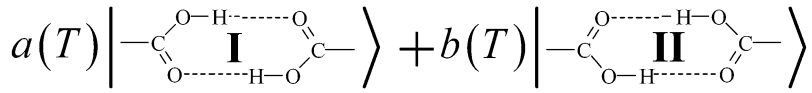

Fig. 2 Sketch of the superposition state of centrosymmetric hydrogen-bonded dimers.

However, experimental evidences for macroscopic coherent tunnelling of protons in the $KHCO_3$ crystal have been reported, along with a theoretical framework for decoherence-free states [10,31–33]. If there is no decoherence, quantum mechanics does not predict any definite dividing line between the quantum (microscopic) and classical (macroscopic) worlds. Then, the formalism of quantum mechanics extrapolated to macroscopic systems leads to conclusions alien to our commonsense intuition [34–38], such as nonlocal proton dynamics, pseudoparticles, quantum entanglement, non-separability, and "super-rigidity". (All these concepts are defined below.)

A serious hurdle on the way to observing macroscopic quantum behaviors is that measurements, in quantum mechanics, are not innocuous and, normally, lead to decoherence [39]. This is the famous paradox of Schrödinger's cat in a superposition of dead and alive states. As soon as it is observed, the cat is either dead or alive and further measurements of the same cat will give the same outcome. The quantum superposition can be observed only if the system is not perturbed in any way by the probe and remains in the same state after the measurement has been completed. We shall see below how such "noninvasive" measurements [40] can be realized. By contrast, Bragg diffraction, NMR, nuclear quadrupole resonance (NQR), QENS, and vibrational spectroscopy are not decoherence-free.

The organization of this paper is as follows. We present the crystal structure of $KHCO_3$ and explain why it offers the best opportunity to observe macroscopic quantum effects. Then, we present an abstract of the theoretical framework for the macroscopic quantum behavior of protons. In the next step, we review neutron-scattering experiments featuring quantum correlations. Finally, Cat-states, interconversion dynamics, and thermal equilibrium are documented.

CRYSTAL STRUCTURE OF $KHCO_3$

The crystal at 14 K is monoclinic, space group $P2_1/a$ (C_{2h}^5), with four $KHCO_3$ entities per unit cell (Fig. 3) [33,41,42]. All protons are crystallographically equivalent and indistinguishable. They are found in planar centrosymmetric dimer entities $(HCO_3^-)_2$ well separated by the stacking of potassium atoms, and linked by moderately strong hydrogen bonds with distances $R_{O\cdots O} \approx 2.6$ Å.

A remarkable feature is that all dimers lie practically in the $(30\bar{1})$ planes and hydrogen bonds are virtually parallel to each other. Single crystals are therefore unique to probe dynamics along specific directions (x,y,z in Fig. 3) parallel to proton modes: stretching (ν OH); in-plane bending (δ OH); and out-of-plane bending (γ OH), respectively.

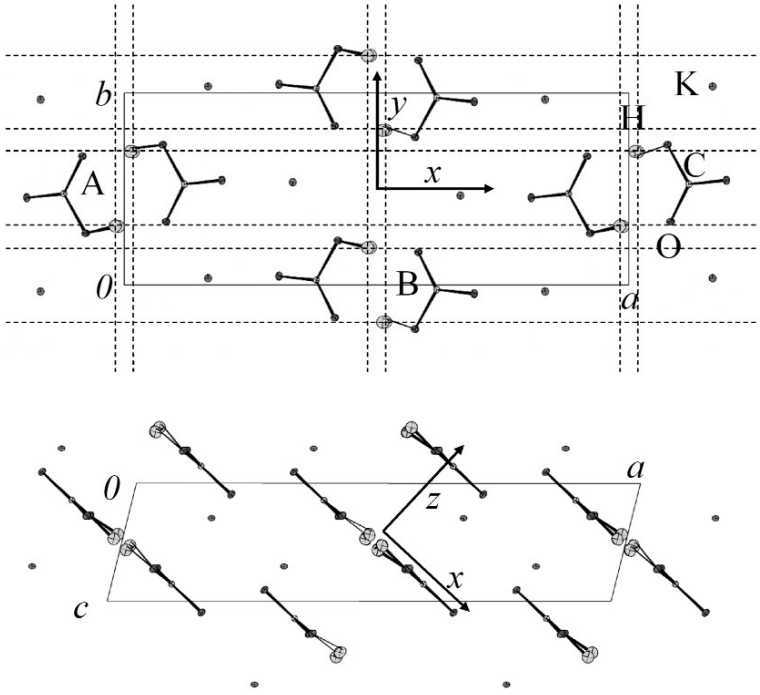

Fig. 3 Schematic view of the crystalline structure of $KHCO_3$ at 14 K. The dashed lines through protons are guides for the eyes.

From 14 to 300 K, the increase of the unit cell dimensions is marginal and there is no phase transition. However, the population of the proton sites changes significantly (Fig. 4). Below ≈150 K, protons are located at a single site (configuration I). At higher temperatures, protons are distributed among two sites at ≈ ±0.3 Å off-center of the hydrogen bond. The center of symmetry is preserved. The secondary proton sites (configuration II) are also crystallographically equivalent and indistinguishable.

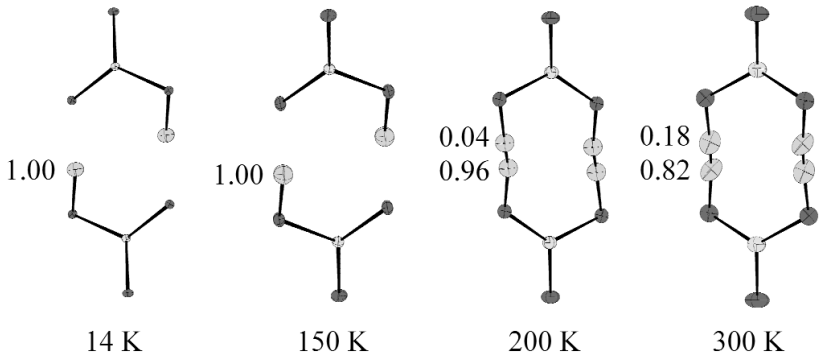

Fig. 4 Probability densities for protons in the $KHCO_3$ crystal at various temperatures.

The sum of the occupancy numbers of the proton sites is unity at any temperature, to within experimental errors. Therefore, proton transfer and interconversion do not destroy the spatial coherence in any way. Otherwise, a significant amount of the coherent scattering should collapse into off-Bragg-peaks diffuse scattering [27,28] and lead to an apparent decrease of the total amount of protons.

The spatial coherence of dimers can be interpreted in different ways. The most intuitive model is a mixture of crystal configurations, say **C1** and **C2**, composed of dimers **T1** and **T2**, respectively, leading to the probability density $\mathbf{C}(T) = a^2(T)\mathbf{C1} + b^2(T)\mathbf{C2}$. In this view, sometimes referred to as "macroscopic realism", a macroscopic system with two or more macroscopically distinct states available to it will at all times be in one or the other of these states [30,40].

Alternatively, the full-blooded quantum mechanical model is a superposition of macroscopic states, say $\overline{|\mathbf{I}\rangle}$ and $\overline{|\mathbf{II}\rangle}$, analogous to states $|\mathbf{I}\rangle$ and $|\mathbf{II}\rangle$ in Fig. 2, respectively, but extended across the whole crystal. Quantum interferences (quantum beats) are expected, if the quantum superposition is decoherence-free. In the next section, we show that the adiabatic separation of proton dynamics leads to such decoherence-free states.

ADIABATIC SEPARATION AND DECOHERENCE-FREE STATES

Within the framework of the Born–Oppenheimer approximation, the vibrational Hamiltonian for a OH···O hydrogen-bonded crystal in the electronic ground state can be partitioned as

$$H = H_H + H_{at} + C_{Hat}, \tag{1}$$

where H_H and H_{at} represent the sublattices of protons (H^+) and heavy atoms, respectively, while C_{Hat} couples the two subsystems. For hydrogen bonds, coupling terms between OH (especially ν OH) and O···O degrees of freedom are rather large [3,43]. In the semiclassical approach, protons are treated as dimensionless particles and the coupling leads to mass renormalization.

Alternatively, the adiabatic separation of the two subsystems is appropriate for quantum dynamics. This separation is justified by the light mass of protons compared to other atoms. It means that, if there is no other damping mechanism, protons in a certain eigen state will remain in the same state in the course of time, while heavy atoms oscillate within adiabatic potentials depending on the proton state

through the coupling terms. This separation holds if there is no crossing of the adiabatic potentials for different proton states.

The adiabatic separation is widely regarded as a relevant approximation for hydrogen bonds like those in $KHCO_3$ or C_6H_5COOH [3]. In fact, the separation is rigorously exact in the ground state. (Obviously, protons will remain in the ground state forever if there is no external perturbation.) The ground state is therefore decoherence-free with respect to heavy atoms, and proton dynamics are those of bare particles (m = 1 amu).

On the other hand, proton transfer along hydrogen bonds and interconversion are strongly coupled to the electronic structure of the dimers. However, the adiabatic separation of electrons and nucleus in the Born–Oppenheimer approximation yields similar conclusions: in the electronic ground state, the bare protons (H^+) are separated from electron dynamics. The coupling is embedded in the adiabatic potential. Needless to say, excited electronic states for the systems under consideration are far beyond the thermal energy range.

PSEUDOPROTONS AND QUANTUM ENTANGLEMENT

In this section, we present a dynamical model composed of two coupled harmonic oscillators in three dimensions for a centrosymmetric proton pair, labelled *j,k,l* with respect to the crystal frame, adiabatically separated from heavy atoms. Coordinates and conjugated moments are α_{1jkl}, P_{1jkl}, and α_{2jkl}, P_{2jkl}, respectively, with $\alpha = x,y,z$. According to textbooks [44], normal coordinates and conjugated moments

$$\left.\begin{aligned} \alpha_{sjkl} &= \frac{1}{\sqrt{2}}\left(\alpha_{1\,jkl} - \alpha_{2\,jkl}\right), \quad P_{sjkl\alpha} = \frac{1}{\sqrt{2}}\left(P_{1\,jkl\alpha} - P_{2\,jkl\alpha}\right), \\ \alpha_{ajkl} &= \frac{1}{\sqrt{2}}\left(\alpha_{1\,jkl} + \alpha_{2\,jkl}\right), \quad P_{ajkl\alpha} = \frac{1}{\sqrt{2}}\left(P_{1\,jkl\alpha} + P_{2\,jkl\alpha}\right), \end{aligned}\right\} \tag{2}$$

split the system into two uncoupled harmonic oscillators at frequencies $\hbar\omega_{sa} = \hbar\omega_{0a}\sqrt{1 + 4\lambda_{0a}}$ and $\hbar\omega_{aa} = \hbar\omega_{0a}$, respectively, each with an effective mass m = 1 amu. Note that the center of symmetry is dictated by the crystal structure, irrespective of the coupling term between the two oscillators, $\lambda_{0\alpha}$.

The Gaussian wave functions of the ground state are $\Psi_0^a(\alpha_{ajkl})$ and $\Psi_0^s(\alpha_{sjkl} \pm \sqrt{2}\alpha_{0\,jkl})$, with equilibrium positions at $\pm\alpha_{0jkl}$. These wave functions are nonlocal and cannot be factored into wave functions for each particle. The particles are entangled in position and momentum, and we cannot assign a definite quantum state to each of them. They are not observables. In addition, since they are indistinguishable, the total wave function must be antisymmetrized with respect to permutation, according to the symmetrization postulate (Pauli principle). For this purpose, we start with linear combinations of $\Psi_0^a(\alpha_{ajkl})\,\Psi_0^s(\alpha_{sjkl} \pm \sqrt{2}\alpha_{0\,jkl})$ either symmetrical or antisymmetrical with respect to proton permutation:

$$\Theta_{0\,jkl\pm} = \frac{1}{\sqrt{2}}\left[\prod_\alpha \Psi_0^a(\alpha_{ajkl})\Psi_0^s(\alpha_{sjkl} - \sqrt{2}\alpha_{0\,jkl}) \pm \prod_\alpha \Psi_0^a(\alpha_{ajkl})\Psi_0^s(\alpha_{sjkl} + \sqrt{2}\alpha_{0\,jkl})\right]. \tag{3}$$

Then, we include the spin symmetry in the antisymmetrized-state vectors [44]

$$\left.\begin{aligned} \left|0\,jkl+\right\rangle &= \left|\Theta_{0\,jkl+}\right\rangle \otimes \frac{1}{\sqrt{2}}\left|\left|\uparrow_1\downarrow_2\right\rangle - \left|\downarrow_1\uparrow_2\right\rangle\right\rangle; \\ \left|0\,jkl-\right\rangle &= \left|\Theta_{0\,jkl-}\right\rangle \otimes \frac{1}{\sqrt{3}}\left|\left|\uparrow_1\uparrow_2\right\rangle + \left|\downarrow_1\downarrow_2\right\rangle + \frac{1}{\sqrt{2}}\left|\uparrow_1\downarrow_2 + \downarrow_1\uparrow_2\right\rangle\right\rangle \end{aligned}\right\} \tag{4}$$

Now, the system is a superposition of fully entangled states in positions, moments, and spins. The Pauli principle, along with the centrosymmetric structure, imposes the singlet- and triplet-like spin symmetry, although, in contrast to magnetic systems [45,46], there is no spin–spin interaction and no energy splitting. This symmetry-related quantum entanglement is energy-free.

Note that the spin symmetry is in conflict with the concept of "local realism" put forward by Einstein, Podolsky, and Rosen (EPR) [34] since it is totally independent of any correlation between nuclear spins (EPR "elements of reality"). Broadly speaking, the entangled pair is different from the sum of its parts.

In quantum mechanics, normal coordinates define nonlocal pseudoprotons, say $\Pi_{sjkl\alpha}$, $\Pi_{ajkl\alpha}$, corresponding to symmetric or antisymmetric displacements of two "half-pseudoparticles". In the ground state, each proton site is a superposition of two such half-pseudoprotons. Only these pseudoprotons are observables, whereas individual positions, moments, and spins of particles are not.

Pseudoprotons become separable in the excited vibrational states at

$$\sum_{\alpha}[(n_{\alpha a}+1/2)\hbar\omega_{\alpha a}+(n_{\alpha s}+1/2)\hbar\omega_{\alpha s}] \tag{5}$$

thanks to the *a*-*s* splitting. The nonlocal dynamics (normal coordinates) is preserved, but the spin symmetry is destroyed.

MACROSCOPIC QUANTUM ENTANGLEMENT AND SUPER-RIGIDITY

Now, we extend the entangled states of a dimer to the sublattice of indistinguishable protons composed of very large numbers (N_a, N_b, N_c, $N = N_aN_bN_c$), of unit cells labelled *j,k,l,* along the crystal axes (*a*), (*b*), (*c*), respectively. For each unit cell, there are two dimer entities (labeled A and B in Fig. 3) related through the (*a*,*c*) glide plane. These dimers are indexed as *jkl* and *j'kl*, respectively, with, not forgetting they are indistinguishable, $j = j'$. At a low temperature, all protons are in configuration **I** (Fig. 3).

Collective dynamics in crystals are normally represented as phonons. Suppose, although this is not the case, proton pairs (eq. 4) could behave as composed bosons analogous to Cooper pairs in superconductors or atom pairs in superfluid ^{3}He [47]. Then, spatially periodic excitations of dimers should be unaffected by pair permutation and could propagate across the lattice [33].

However, this is impossible for $KHCO_3$ because protons are not paired. The elementary entity in the crystal structure is the monomer $KHCO_3$, not the dimer $(KHCO_3)_2$. Therefore, there is no "bosonization", and collective dynamics must be antisymmetrized upon interchange of any two protons, wherever located in the crystal. Such permutations applied to plane waves merely change the signs of the phases, and superposition of these antiphase waves automatically yields zero amplitude. Hence, phonons are forbidden. The proton sublattice has no internal dynamics and can be termed "super-rigid". This macroscopic quantum behavior does not depend in any way on local interactions between protons. It is dictated exclusively by the translational symmetry of the lattice.

Now, we realize that if proton sites are indistinguishable and if any state must be antisymmetrized with respect to any permutation, then, normal coordinates (eq. 2) and state vectors (eq. 4) are not localized at any particular unit cell *j,k,l*. Their nonlocal nature is extended throughout the crystal and must be represented as linear combinations of the state vectors (eq. 4)

$$\left|0\tau\right\rangle = \frac{1}{\sqrt{N}}\left|\sum_{l=1}^{N_c}\sum_{k=1}^{N_b}\sum_{j=j'=1}^{N_a}\left[\left|0jkl\tau\right\rangle+\left|0j'kl\tau\right\rangle\right]\right\rangle \tag{6}$$

Here, τ = "+" or "–" for singlet- or triplet-like spin symmetry, respectively. Then, the local coordinates are totally hidden and any permutation is meaningless. These nonlocal states avoid any conflict with the

symmetrization postulate. They represent macroscopic single-pseudoproton states with the occupation number of 1/(2*N*) pseudoprotons per site. The wave functions

$$\Theta_{0\tau} = \frac{1}{\sqrt{N}} \sum_{l=1}^{N_c} \sum_{k=1}^{N_b} \sum_{j=j'=1}^{N_a} \left[\Theta_{0\,jkl\tau} + \Theta_{0\,j'kl\tau} \right] \tag{7}$$

describe the recoil of a super-rigid pseudoproton as a whole. The wave functions oscillate synchronously in-phase throughout the crystal.

The sublattice is a superposition of 2*N* degenerate macroscopic pseudoproton states:

$$\overline{|0\rangle} = \sqrt{N} \sum_{\tau} |0\tau\rangle \tag{8}$$

Each pseudoproton is evenly distributed over all sites, and each site is equally occupied by the same fractional number of all pseudoprotons, in such a way that the total occupation number at each site is equivalent to one proton. The macroscopic wave function

$$\overline{\Theta_0} = \sqrt{N} \sum_{\tau} \Theta_{0\tau} \tag{9}$$

represents the recoil of the whole superlattice. These nonlocal states are macroscopically entangled. To the best of our knowledge, there has been no other example of a super-rigid lattice ever reported.

The adiabatic separation ensures that the super-rigid lattice is decoherence-free with respect to heavy atoms. Moreover, although photons, neutrons, etc., may single-out some disentangled pseudoproton states, energy-free re-entanglement occurs automatically after decay to the ground state, by virtue of indistinguishability. Massive decoherence is therefore avoided. Re-entanglement on the timescale of proton dynamics (~10^{-13}–10^{-14} s) allows the sublattice to be in thermal equilibrium with the surroundings, despite the lack of internal dynamics. The sublattice of protons can thus adjust to structural changes, for example with temperature and pressure.

Among many paradoxical properties, the super-rigidity is simultaneously extremely robust, thanks to spontaneous energy free re-entanglement, and very fragile since it is not stabilized by any energy gain. Even elastic perturbations can transiently disrupt the super-rigidity.

For the deuterated analog, $KDCO_3$, eqs. 4 and 6 are irrelevant for bosons. The ground-state wave function for dimers

$$\Theta_{0\,jkl} = \prod_{\alpha} \Psi_0^a(\alpha_{ajkl}) \Psi_0^s(\alpha_{sjkl} \pm \sqrt{2}\alpha_{0\,jkl}) \tag{10}$$

is unaffected by permutation and spin correlation is not required. Dynamics are represented as nonlocal pseudodeuterons, and phonons are allowed. State vectors analogous to eq. 6 can be rewritten as

$$|0s\rangle = \frac{1}{\sqrt{N}} \left| \sum_{l=1}^{N_c} \sum_{k=1}^{N_b} \sum_{j=j'=1}^{N_a} \left[|0\,jkl\rangle + s\,|0\,j'kl\rangle \right] \exp i\left(j\varphi_a + k\varphi_b + l\varphi_c \right) \right\rangle \tag{11}$$

where φ_a, φ_b, φ_c, are phase angles along the axes (*a*), (*b*), (*c*), respectively, and $s = \pm 1$. Needless to say, the numbers of degrees of freedom are identical for the two systems.

POTENTIAL FUNCTION FOR PROTON TRANSFER

In order to rationalize temperature effects, we need to model proton-transfer dynamics. Vibrational spectra (infrared, Raman, and INS) converge to a quasi-symmetric double minimum potential for proton transfer along the OH stretching coordinate *x* (Fig. 5). The shape is dictated entirely by experimen-

tal data. The distance between the minima ($2x_0 \approx 0.6$ Å) is known from the crystal structure. The upper states at $h\nu_{02}$ and $h\nu_{03}$ were determined from the band-shapes of the ν OH modes in the infrared and Raman [13,14]. The ground-state splitting ($h\nu_{01} \approx 216$ cm^{-1}) was determined with INS, thanks to the large scattering cross-section of protons [17,48]. If the potential were symmetrical, the splitting of the ground state (the tunnelling frequency) would be $h\nu_{0t} \approx 18$ cm^{-1}. The observed 0–1 splitting is therefore largely representative of the potential asymmetry.

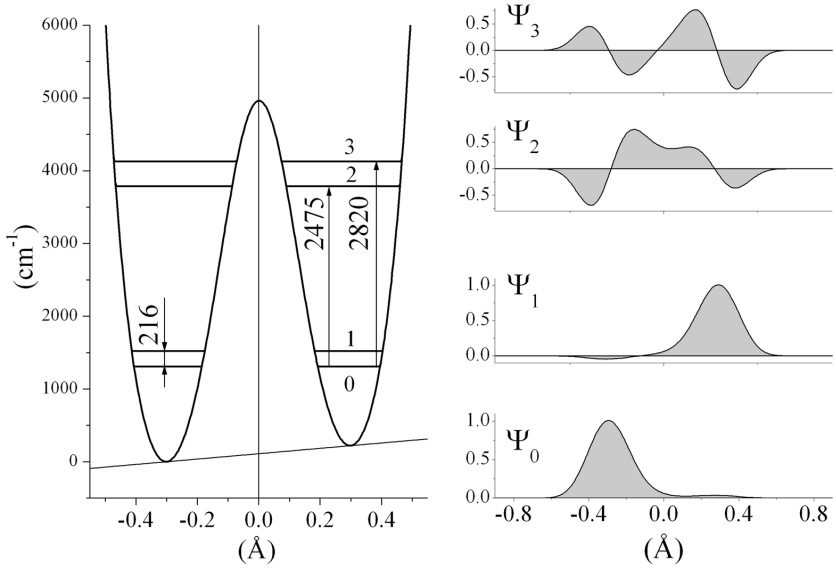

Fig. 5 Potential function and wave functions for the OH stretching mode along the hydrogen bond in the $KHCO_3$ crystal. The oscillator mass is 1 amu.

The wave functions in the $|0\rangle$ and $|1\rangle$ states are largely localized in the lower and upper wells, respectively (Fig. 5). A small fraction ($\varepsilon \approx 0.05$) is delocalized in the other well, but, needless to say, the tiny delocalization of the probability density is not visible in Fig. 3. Although very small, ε plays a key role in spectroscopy and proton-transfer dynamics.

This potential has been a puzzle ever since it was determined, because it was naively thought to be representative of the non-centrosymmetric transfer of a single bare proton within a dimer, leading to unrealistic di- and de-protonated carbonate ions. This dynamics should destroy the center of symmetry and cancel out the selection rules for infrared and Raman. However, this is not observed.

We now understand that if pseudoprotons are the observables, instead of local protons, this potential is a nonlocal potential for the transfer of a macroscopic pseudoproton. The proton configurations in the tunnelling states are sketched in Fig. 6. The ground state corresponds to the structure observed at low temperature (Fig. 3). The state at $h\nu_{01}$ corresponds to the transfer of a pseudoproton (either Π_a or Π_s) to the unoccupied sites. Then, the state corresponding to the transfer of a further pseudoproton should be at $2h\nu_{01}$. (The pseudoprotons are uncoupled by definition.)

The tiny delocalization of the wave functions over the two wells does not change the conclusion that pseudoprotons in the ground state are nonseparable. The sublattice is fully entangled, and spin symmetry is pertinent. It is therefore possible to define the fully entangled tunnelling states $|\overline{\mathbf{I}}\rangle$ (ground state) and $|\overline{\mathbf{II}}\rangle$ (at $2h\nu_{01}$) analogous to eq. 7. On the other hand, the intermediate state $|\mathbf{V}\rangle = 2^{-1/2}$ $[|\mathbf{II}_a\rangle \otimes |\mathbf{I}_s\rangle \pm |\mathbf{I}_a\rangle \otimes |\mathbf{II}_s\rangle]$ representing separated pseudoprotons is twofold degenerate, with no definite

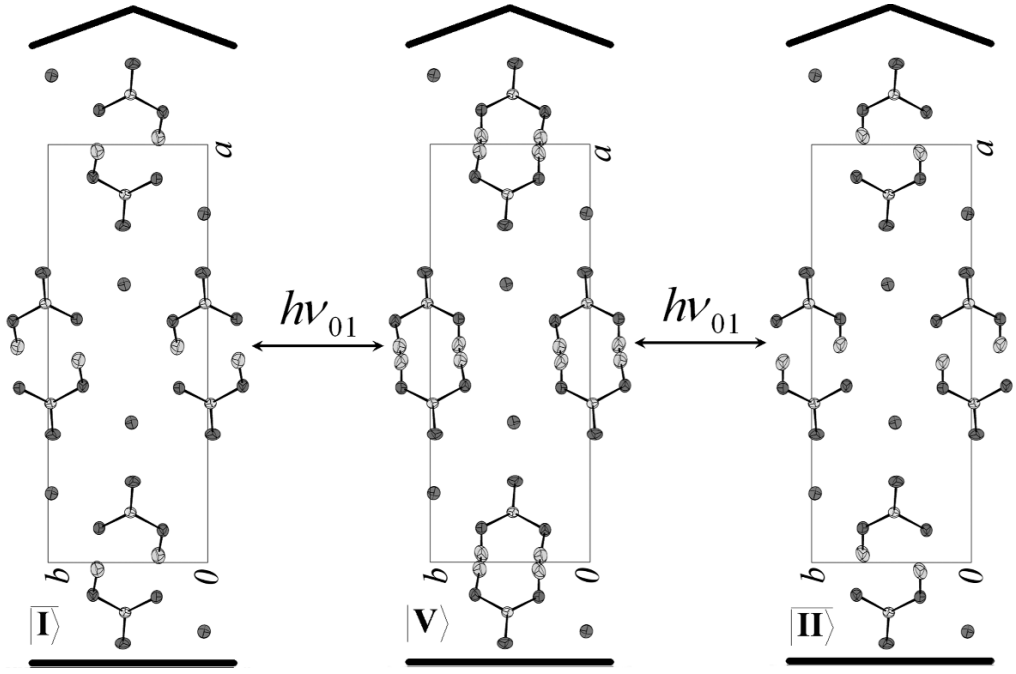

Fig. 6 Schematic view of the proton configurations for the tunnelling states. The ground state $\overline{|\mathbf{I}\rangle}$ and the upper state $\overline{|\mathbf{II}\rangle}$ at $2h\nu_{01}$ are fully entangled. The intermediate virtual state $|\mathbf{V}\rangle$ at $h\nu_{01}$ is disentangled. All proton sites are equally occupied.

spin symmetry. We will show below that this virtual state does not contribute to the proton population at thermal equilibrium.

TEMPERATURE EFFECTS

Since the probability for simultaneous transfer of two pseudoprotons is extremely small, the interconversion dynamics is essentially a two-stepwise process, each step corresponding to the transfer of a pseudoproton preserving the center of symmetry. In the first step, energy transfer $\pm h\nu_{01}$ singles out a superposition of pseudoprotons in the $|\mathbf{V}\rangle$ state

$$\overline{|\mathbf{I}\rangle} \xrightarrow{+h\nu_{01}} |\mathbf{V}\rangle \xleftarrow{-h\nu_{01}} \overline{|\mathbf{II}\rangle} \tag{12}$$

The second step is energy-free re-entanglement

$$|\mathbf{V}\rangle \longleftrightarrow 2^{-1/2}\left[\overline{|\mathbf{I}\rangle} \pm \overline{|\mathbf{II}\rangle}\right] \tag{13}$$

This interconversion mechanism allows the entangled states to be in thermal equilibrium. The population of the secondary proton site is

$$P(T) = 2p_{01}^2(T)[1 + p_{01}^2(T)]^{-1} \tag{14}$$

with $p_{01}(T) = \exp(-h\nu_{01}/kT)$. In Fig. 7, the solid line is in reasonable agreement with measurements.

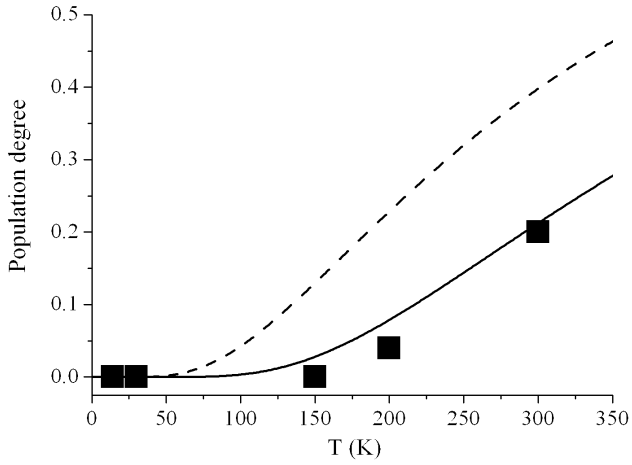

Fig. 7 Population degrees of the secondary proton sites as a function of temperature. ■: experiments. Solid line: eq. 14 for entangled states. Dashed line: eq. 15 for disentangled states.

Alternatively, for disentangled states in thermal equilibrium, the population would be

$$P'(T) = \left[p_{01}(T) + 2p_{01}^2(T) \right][1 + p_{01}(T) + p_{01}^2(T)]^{-1} \tag{15}$$

The dashed curve in Fig. 7 is quite at variance with measurements. Clearly, the population degree of the intermediate states does not obey Boltzmann's law. Presumably, the life-time of these states is too short to contribute significantly to neutron diffraction.

The curves in Fig. 7 accord with a thermal equilibrium of the macroscopically entangled tunnelling states, but the probability densities do not allow us to decide whether the crystal is a superposition or a mixture of these states. Further information on the quantum coherence can be obtained as follows. For a quantum superposition of the entangled states, the pseudoproton state should be as

$$\left|\Psi(T,\tau)\right\rangle = \frac{1}{\sqrt{N}} \left| \sum_{l=1}^{N_c} \sum_{k=1}^{N_b} \sum_{j=j'=1}^{N_a} \left\{ a(T)\left[\left|0jkl\tau\right\rangle + \left|0j'kl\tau\right\rangle \right] + b(T)\left[\left|1jkl\tau\right\rangle + \left|1j'kl\tau\right\rangle \right] \right\} \right\rangle \tag{16}$$

with $b^2(T) = 1 - a^2(T) = p^2{}_{01}/[1 + p^2{}_{01}]$. The crystal state should be then

$$\overline{\left|\Psi(T)\right\rangle} = \sqrt{N} \sum_{\tau} \left|\Psi(T,\tau)\right\rangle = \sqrt{N} \sum_{\tau} \left[a(T)\left|\mathbf{I}\tau\right\rangle + b(T)\left|\mathbf{II}\tau\right\rangle \right] \tag{17}$$

where $|\mathbf{I}\tau\rangle$ and $|\mathbf{II}\tau\rangle$ are analogous to eq. 8. Alternatively, for a statistical mixture, each pseudoproton is in one state $|\mathbf{I}\tau\rangle$ or the other $|\mathbf{II}\tau'\rangle$, as

$$\overline{\left|\Psi'(T)\right\rangle} = \sqrt{N} \left[a(T) \sum_{\tau} \left|\mathbf{I}\tau\right\rangle + b(T) \sum_{\tau'} \left|\mathbf{II}\tau'\right\rangle \right] \tag{18}$$

Compared to eq. 16, the spin symmetry is no longer a relevant quantum number.

PROBING QUANTUM ENTANGLEMENT WITH NEUTRONS

In this section, we examine how noninvasive measurements with neutrons can probe macroscopic quantum entanglement. We shall use the following definitions. The incident and scattered wave vectors are

$\mathbf{k_0}$ and $\mathbf{k_f}$, respectively, with $|\mathbf{k_0}| = 2\pi/\lambda_0$ and $|\mathbf{k_f}| = 2\pi/\lambda_f$. The momentum transfer vector is $\mathbf{Q} = \mathbf{k_0} - \mathbf{k_f}$. Q_x, Q_y, Q_z, are projections onto the x,y,z, axes, respectively (Fig. 3).

The advantages of neutrons, compared to other probes, are as follows. First, neutrons, contrary to photons, can probe vibrational dynamics in the ground state, through elastic scattering. This is a prerequisite to evidence the super-rigidity of the proton sublattice. Second, the spin symmetry of macroscopic states increases dramatically the coherent scattering cross-section of protons from ≈1.8 to ≈82.0 barns [27]. Third, the high flux of epithermal neutrons available at advanced spallation sources provides the most detailed view over the reciprocal space. Finally, as the transversal coherence length of a neutron beam emitted by a remote source is about the beam section (≈10 cm^2), macroscopic quantum effects can be probed on a large scale. Neutron scattering can be decomposed into distinct events.

First, Bragg peaks at nodes of the reciprocal lattice. Except for very particular orientations of **Q**, momentum transfer destroys the spin symmetry and super-rigidity. Only probability densities are measured, and it is impossible to distinguish superposition states or mixtures.

Second, incoherent scattering, essentially by protons, gives an anisotropic continuum of intensity centered at $\mathbf{Q} = 0$. Here, energy and momentum transfer destroy the spin symmetry. Only for elastic scattering, the spin symmetry of the initial and final states of decorrelated dimers (eq. 4) is preserved and quantum interferences can be observed [32].

Third, the conditions for noninvasive measurements (no energy or kinetic momentum transfer and no spin flip) are realized when at least one of the components Q_x, Q_y, or Q_z corresponds to a node of the reciprocal super-rigid lattice. Then, the momentum transfer vector is the same at all proton sites along the matching directions and neutrons probe the recoil of the super-rigid lattice as a whole, without any perturbation of its internal state. Even if the spin symmetries of the initial and final states are different ($\tau_i \neq \tau_f$), there is no "real" proton-spin flip and no measurement-induced decoherence. (In fact, transitions $\tau_i \leftrightarrow \tau_f$ are not separable.) We anticipate dramatically enhanced intensity for these scattering events [10,33].

In the particular case of $KHCO_3$, neutron-scattering events by entangled protons can be rationalized as follows. First, protons in dimer planes aligned along directions parallel to y (dotted lines in Fig. 3) are equivalent to double lines of scatterers separated by $2x_0$, with some similarity to Young's double slits. Second, neutron diffraction by the coherent structures in two dimensions (quantum arrays) composed of double lines parallel to dimer planes gives rods of diffuse scattering parallel to Q_z, effectively observed for particular values of Q_x and Q_y [10,33]. Finally, for **Q**-values at the nodes of the reciprocal superlattice, totally coherent elastic scattering gives diffraction peaks with enhanced intensities due to the spin symmetry.

Quantum double slits

Consider an alignment of entangled proton pairs, say along (*b*) (one of those emphasized in Fig. 3). Similar double lines can be seen along (*a*) and (*c*) axes. For momentum transfer Q_x ($Q_y = Q_z = 0$), each double line behaves as an ensemble of entangled pairs (eq. 4). The elastic scattering function is

$$S_{jkl}(Q_\alpha, \omega_\alpha) = \sum_{\tau_i, \tau_f} \left| \left\langle 0\, jkl\, \tau_f \left| \exp iQ_\alpha \left(\alpha_{1jkl} - \alpha_{0jkL} \right) + \tau_f \tau_i \exp iQ_\alpha \left(\alpha_{1jkl} + \alpha_{0jkL} \right) \right| 0\, jkl\, \tau_i \right\rangle \right.$$
$$\left. \times \left\langle 0\, jkl\, \tau_f \left| \exp iQ_\alpha \left(\alpha_{2jkl} - \alpha_{0jkL} \right) + \tau_f \tau_i \exp iQ_\alpha \left(\alpha_{2jkl} + \alpha_{0jkL} \right) \right| 0\, jkl\, \tau_i \right\rangle \right|^2 \quad (19)$$
$$\times \delta(\omega_\alpha)$$

The initial and final states are $|0\, jkl\, \tau_i\rangle$ and $|0\, jkl\, \tau_f\rangle$, respectively. The product of two brackets accounts for the lack of definiteness of the scattering center: Neutrons are scattered simultaneously by the two nonseparable pseudoprotons with definite spin symmetry (Π_a, Π_s), each of them being simultaneously

at both sites. Neutrons are scattered in-phase for $|\pm\rangle \longleftrightarrow |\pm\rangle$ ($\tau_f\tau_i = +1$), or antiphase for $|\pm\rangle \longleftrightarrow |\mp\rangle$ ($\tau_f\tau_i = -1$) . The scattering function can be rewritten as [31,32]

$$\left.\begin{aligned} S_{\pm\pm}\left(Q_\alpha,\omega_\alpha\right) &= \cos^4\left(Q_\alpha\alpha_0\right)\left[\exp-\frac{Q_\alpha^2 u_{0\alpha}^2}{\sqrt{1+4\lambda_\alpha}}+\exp-Q_\alpha^2 u_{0\alpha}^2\right]\delta(\omega_\alpha)\\ S_{\pm\mp}\left(Q_\alpha,\omega_\alpha\right) &= 2\sin^4\left(Q_\alpha\alpha_0\right)\exp\left[-Q_\alpha^2\left(\frac{u_{0\alpha}^2}{2\sqrt{1+4\lambda_\alpha}}+\frac{u_{0\alpha}^2}{2}\right)\right]\delta(\omega_\alpha)\end{aligned}\right\} \quad (20)$$

Here, $u_{0\alpha}^2 = \hbar/(2m\omega_{0\alpha})$ is the mean square amplitude in the ground state for uncoupled harmonic oscillators. In the weak coupling limit relevant for $KHCO_3$ ($4\lambda_{0\alpha} = 1$), the virtually identical Gaussian profiles are modulated by interference fringes proportional to $[\cos^4(Q_\alpha\alpha_0) + \sin^4(Q_\alpha\alpha_0)]$ (Fig. 8a).

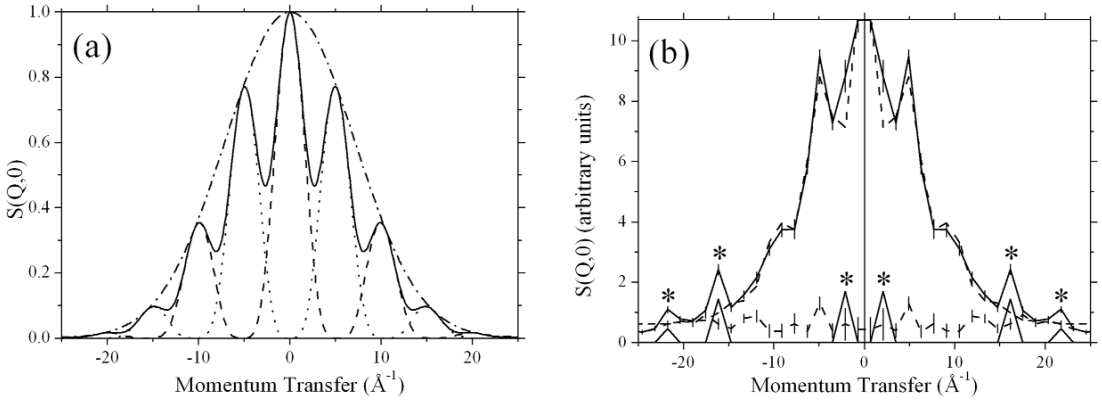

Fig. 8 (a) Comparison of the theoretical profiles $\boldsymbol{S(Q_\alpha,0)}$ for a nonentangled pair (dot-dash), and for a coupled pair of fermions, according to eq. 20 (solid line). The dot-and-dash curves represent interference fringes for in-phase and out-of-phase neutron scattering. (b) $\boldsymbol{S(Q_y,0)}$ measured at 20 K for a single crystal of $KHCO_3$ (solid curve with error bars). Comparison with the best fit (dashed line) obtained with eq. 20 convoluted with a triangular resolution function. The dashed line with error bars is the difference spectrum. Triangular functions (*) were attributed to other scattering processes.

Such interference fringes were effectively observed for $KHCO_3$ at 20 K with the MARI spectrometer [49] at the ISIS pulsed-neutron source (Fig. 8b) [32,50]. Best-fit exercises yield double-line separations in reasonable accordance with the crystal structure, and the oscillator mass estimated from $u_{0\alpha}^2$ is virtually equal to 1 amu. Disentangled pairs would give Gaussian profiles (Fig. 8a), at variance with observations. These experiments are, therefore, positive evidence that proton states in dimers are fully entangled with definite spin symmetry (eq. 4).

In contrast to experiments conducted with classical double slits [53–55], questions such as "which-way?" or "which-slit?" are pointless in the present context. Each neutron is scattered simultaneously at both sites, and it is impossible to fire at will one proton or the other. Interpretative models based on "local" coordinates or spins [51,52] can be excluded.

Quantum array

For noninvasive diffraction by a superposition state (eq. 17) of the super-rigid arrays in two dimensions, Q_x and Q_y should correspond to nodes of the reciprocal superlattice, while Q_z is a free parameter for in-

coherent scattering. The differential cross-section gives cigar-like rods of diffuse scattering along Q_z, parallel to (a*,c*) planes. (The scattering cross-section and the positions of the rods can be found in ref. [10]). The profile of intensity along Q_z is proportional to the Debye–Waller factor "exp(-2W_z)". It is rather broad at low temperatures and narrows rapidly at elevated temperatures, thanks to the thermal population of the density-of-states.

Super-rigid crystal

The differential cross-section for the super-rigid lattice in three dimensions diverges along the previous rods of intensity at $Q_z = \pm n_z 2\pi D_z$, with $2\pi D_z \approx 1.92$ Å^{-1} [10]. For these peaks, the crystal cross-section (≈101.7 barns) is much greater than that for regular Bragg peaks (≈21.7 barns). Moreover, as there is no Debye–Waller factor for a super-rigid lattice, enhanced peaks prevail over regular Bragg peaks at elevated temperatures, especially at large |**Q**|-values. In addition, as the proton lattices in the tunnelling states $\overline{|\mathbf{I}\rangle}$ and $\overline{|\mathbf{II}\rangle}$ (Fig. 6) are crystallographically identical, the peak positions are temperature-independent.

Neutron diffraction experiments

With the time-of-flight instrument SXD [56] at ISIS, one can measure at once large domains of the reciprocal space. A complete set of data has been presented in ref. [10]. Only cuts in the (a*,c*) planes measured at 30 and 300 K are presented in Fig. 9.

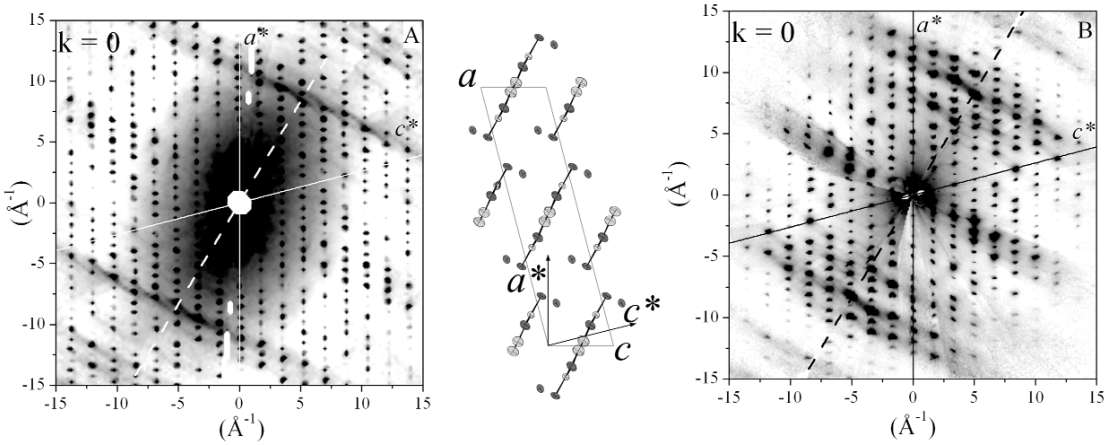

Fig. 9 Diffraction patterns of $KHCO_3$ at 30 K (A) and 300 K (B) in the (a*,c*) plane. The ridges of intensity at Q_x = **0** and ≈ ± **10** Å^{-1} from the origin lie along a direction parallel to Q_z, and as such are perpendicular to the plane of dimers (dashed lines along Q_x). The insert visualizes the correspondence between the direct and reciprocal lattices.

At 30 K (Fig. 9A), the lines of diffuse scattering due to quantum entanglement are clearly visible, in addition to Bragg peaks and to the anisotropic continuum of intensity, centered at Q = 0, due to incoherent scattering. (Note that in contrast to the MARI experiments in Fig. 8, scattered neutrons were collected without any energy discrimination and inelastic scattering events hide the interference fringes specific to elastic scattering.) These lines of intensity have all the characteristics anticipated for diffraction by the quantum arrays of entangled protons: (i) they are clearly separated from Bragg peaks; (ii) their orientations correspond to momentum transfer perpendicular to dimer planes (dashed lines); (iii) positions at $Q_x = \pm$ (10.25 ± 0.25) Å^{-1} along the dashed lines are in accordance with the spacing

of double lines of protons ($2x_0 \approx 0.6$ Å); (iv) the width along (b^*) is similar to that of Bragg peaks (cigar-like shape); (v) the profile of intensity along the ridges is similar to a cut along Q_z of the incoherent scattering centered at $Q = 0$; and (vi) the rods are no longer observed for bosons ($KDCO_3$) [33] (no spin symmetry).

At 300 K (Fig. 9B), regular Bragg peaks and incoherent scattering are largely depressed at large $|\mathbf{Q}|$-values, a normal consequence of the increased population of the lattice density-of-states. Quite remarkably, the lines of intensity are still clearly observed, although the breadth of the diffuse scattering along Q_z is also significantly decreased. In fact, the enhanced Bragg peaks due to the super-rigid lattice are better visible, since they are not attenuated by any Debye–Waller factor. Quantum entanglement remains largely decoherence-free even at elevated temperatures.

Note that even at room temperature, the population of the lowest disentangled state (γ OH $\approx$ 1000 cm^{-1}) remains small (~10^{-2}) and the thermally induced decoherence is marginal.

CAT STATES

Neutron-scattering experiments concur to the conclusion that macroscopic quantum entanglement is intrinsic to the $KHCO_3$ crystal. Although it would be presumptuous to pretend there is no possible alternative interpretation, at the present time of writing we are not aware of any and can state that neutrons entangled with proton states give rise to quantum interferences which cannot be rationalized with models based on "local" particles.

The diffraction pattern at 300 K is positive evidence that the crystal is in a quantum superposition (eq. 17) of macroscopically distinct states like Schrödinger's cat. This result is at variance with the quantum measurement paradox stating that a macroscopic object may be in a linear superposition of states corresponding to macroscopically different behaviors, provided that it is not observed. As opposed to this, we do observe/measure a superposition of macroscopic tunnelling states without any internal perturbation and, therefore, without any induced decoherence.

However, the definition of "macroscopically distinct" states or behaviors [30] is rather ambiguous for $KHCO_3$: The tunnelling states are obviously distinct in the direct space of atom positions, but they are identical in the reciprocal space. This degeneracy is necessary to evidence superposition states. Otherwise, each state could be probed separately and the superposition would be unobservable.

In fact, the superposition state is an objective reality dictated by the crystal structure. The transition from quantum to classical is forbidden by spontaneous re-entanglement. Figure 7 emphasizes that entangled states play an essential role in the evolution of a large ensemble of particles, on the order of Avogadro's constant, in a complex system, even at room temperature.

BENZOIC ACID CRYSTAL

The nearly planar centrosymmetric dimers (C_i) of C_6H_5COOH in the crystal are linked by OH···O hydrogen bonds, with O···O ≈ 2.61 Å, very similar to those in $KHCO_3$. The crystal is monoclinic, $P2_1/c$ (C_{2h}^5) with four crystallographically equivalent C_6H_5COOH entities in the unit cell, and there is no phase transition up to 300 K, while thermally activated interconversion is observed [8,9]. All protons are crystallographically equivalent.

There is no reason to question the adiabatic separation of proton dynamics from heavy atoms and from electrons [25]. Therefore, we expect decoherence-free macroscopic quantum entanglement to occur. However, in contrast to $KHCO_3$, dimers are not parallel to the same planes and the location of enhanced diffraction features should be quite different. Neutron diffraction experiments, in the future, should shed further light on the interplay of the expected super-properties and the crystal structure.

CONCLUSION

Prominent features of quantum mechanics, like quantum entanglement and superposition states, extrapolated from the microscopic level of atoms and molecules to the macroscopic scale of our everyday world are totally alien to commonsense. For open systems, environment-induced decoherence can bring about the transition from quantum to classical behaviors. However, the theory does not predict any definite dividing line between the two regimes and leaves open questions of fundamental importance.

- Is there any upper limit in size, complexity, and temperature for a system to display quantum entanglement?
- How to probe macroscopic quantum entanglement without measurement-induced decoherence?
- Is it possible that superposition states could survive at a macroscopic level in the condensed matter?
- Is it true that some correlations of a macroscopic ensemble cannot be rationalized with definite local properties of the individual constituents?

These questions, and many more, have haunted quantum mechanics ever since it was formulated. The theoretical and experimental evidences presented in this review provide provisional answers to these pending questions, and some others.

The starting point is to recognize that the adiabatic separation of proton dynamics from electrons and heavy atoms in hydrogen-bonded crystals leads to decoherence-free macroscopic states. As long as this separation holds, there is no upper limit in size, complexity, and temperature for macroscopic quantum entanglement.

The key to success in seeking macroscopic quantum effects in crystalline solids is to conduct noninvasive experiments with neutrons to probe many-particle quantum correlations without any perturbation. As a matter of fact, the following conclusions apply to the $KHCO_3$ crystal:

- The sublattice of protons is a macroscopic quantum object on the scale of Avogadro's constant and cm^3. There is no limitation in size, apart from the crystal dimensions. There is no evidence for any transition from quantum to classical regime.
- Neutron diffraction can probe the super-rigid lattice without any perturbation of its internal states.
- The sublattice is a superposition of tunnelling states with macroscopically distinct crystal structures.
- Macroscopic quantum entanglement leads to correlations in conflict with the concept of local reality. The super-rigidity is not due to any local interaction, and the spin symmetry of proton states is not due to any interaction between nuclear spins.

In addition, the super-rigidity of proton states adds a crystalline solid at room temperature to the list of substances with "super" properties due to macroscopic quantum behaviors: liquids (superfluidity in ^{4}He and ^{3}He); vapor (Bose–Einstein condensates of ultracold atoms); and electrons (superconductivity in metals and high-T_c copper oxides) [57].

Last but not least, the interconversion of protons is ruled by two macroscopically coherent mechanisms. On the one hand, the superposition of tunnelling states gives rise, through quantum beats, to coherent oscillations with tiny amplitudes of the probability density for the two tautomeric forms. On the other hand, energy-transfer-induced disentanglement creates a transient state that does not contribute to the thermodynamics, although it is necessary to reach thermal equilibrium.

The theoretical framework for macroscopic quantum entanglement is not specific to the particular case of $KHCO_3$, and we do not see any objection to observing similar dynamics in various hydrogen-bonded crystals. Neutron diffraction studies of such crystals should lead to a deep view of the complex interplay between quantum dynamics and structural-phase transitions.

REFERENCES

1. L. Pauling. *The Nature of the Chemical Bond*, Cornell University Press, Ithaca, NY (1960).
2. S. N. Vinogradov, R. H. Linnell. *Hydrogen Bonding*, Van Nostrand-Reinhold, New York (1971).
3. P. Schuster, G. Zundel, C. Sandorfy. *The Hydrogen Bond. Recent Developments in Theory and Experiments*, Vols. I–III, North-Holland, Amsterdam (1976).
4. P. Schuster. *Hydrogen Bonds*, Springer-Verlag, Berlin (1984).
5. G. A. Jeffrey, W. Saenger. *Hydrogen Bonding in Biological Structures*, Springer-Verlag, Berlin (1991).
6. C. L. Perrin, J. B. Nielson. *Annu. Rev. Phys. Chem.* **48**, 511 (1997).
7. S. Scheiner. *Hydrogen Bonding: A Theoretical Perspective*, Oxford University Press, Oxford (1997).
8. C. C. Wilson, N. Shankland, A. J. Florence. *Chem. Phys. Lett.* **253**, 103 (1996).
9. C. C. Wilson, N. Shankland, A. J. Florence. *J. Chem. Soc., Faraday Trans.* **92**, 5051 (1996).
10. F. Fillaux, A. Cousson, M. J. Gutmann. *J. Phys.: Cond. Matter* **18**, 3229 (2006).
11. R. Graf, R. Meyer, T.-K. Ha, R. R. Ernst. *J. Chem. Phys.* **75**, 2914 (1981).
12. B. H. Meier, F. Graf, R. R. Ernst. *J. Chem. Phys.* **76**, 767 (1982).
13. F. Fillaux. *Chem. Phys.* **74**, 395 (1983).
14. F. Fillaux. *Chem. Phys.* **74**, 405 (1983).
15. S. Benz, U. Haeberlen, J. Tegenfeldt. *J. Magn. Res.* **66**, 125 (1986).
16. R. Meyer, R. R. Ernst. *J. Chem. Phys.* **86**, 784 (1987).
17. F. Fillaux, J. Tomkinson, J. Penfold. *Chem. Phys.* **124**, 425 (1988).
18. J. L. Skinner, H. P. Trommsdorff. *J. Chem. Phys.* **89**, 897 (1988).
19. A. Stöckli, B. H. Meier, R. Kreis, R. Meyer, R. R. Ernst. *J. Chem. Phys.* **93**, 1502 (1990).
20. F. Fillaux, J. Tomkinson. *J. Mol. Struct.* **270**, 339 (1992).
21. G. Eckold, H. Grimm, M. Stein-Arsic. *Physica B* **180–181**, 336 (1992).
22. A. J. Horsewill, D. F. Brougham, R. I. Jenkinson, C. J. McGloin, H. P. Trommsdorff, M. R. Johnson. *Ber. Bunsenges. Phys. Chem.* **102**, 317 (1998).
23. M. Neumann, D. F. Brougham, C. J. McGloin, M. R. Johnson, A. J. Horsewill, H. P. Trommsdorff. *J. Chem. Phys.* **109**, 7300 (1998).
24. F. Fillaux. *Int. Rev. Phys. Chem.* **19**, 553 (2000).
25. F. Fillaux, M.-H. Limage, F. Romain. *Chem. Phys.* **276**, 181 (2002).
26. C. Odin. *J. Phys. Chem. B* **108**, 7402 (2004).
27. S. W. Lovesey. *Nuclear Scattering, Theory of Neutron Scattered from Condensed Matter*, Vol. I, Clarendon Press, Oxford (1984).
28. V. M. Nield, D. A Keen. *Diffuse Neutron Scattering from Crystalline Materials*, Vol. 14 of *Oxford series on neutron scattering in condensed matter*, Clarendon Press, Oxford (2001).
29. F. Fillaux. *Chem. Phys. Lett.* **408**, 302 (2005).
30. A. J. Leggett. *J. Phys.: Condens. Matter* **14**, R415 (2002).
31. F. Fillaux. *Physica D* **113**, 172 (1998).
32. S. Ikeda, F. Fillaux. *Phys. Rev. B* **59**, 4134 (1999).
33. F. Fillaux, A. Cousson, D. Keen. *Phys. Rev. B* **67**, 054301 and 189901(E) (2003).
34. A. Einstein, B. Podolsky, N. Rosen. *Phys. Rev.* **47**, 777 (1935).
35. C. A. Kocher, E. D. Commins. *Phys. Rev. Lett.* **18**, 575 (1967).
36. S. J. Freedman, J. F. Clauser. *Phys. Rev. Lett.* **28**, 938 (1972).
37. J. S. Bell. *Physics Long Island City, N.Y.* **1**, 195 (1964).
38. A. Aspect, P. Grangier, G. Roger. *Phys. Rev. Lett.* **47**, 460 (1981).
39. A. J. Leggett. *Science* **307**, 871 (2005).
40. A. J. Leggett, A. Garg. *Phys. Rev. Lett.* **54**, 857 (1985).
41. J. O. Thomas, R. Tellegren, I. Olovsson. *Acta Crystallogr., Sect. B* **30**, 1155 (1974).

42. J. O. Thomas, R. Tellegren, I. Olovsson. *Acta Crystallogr., Sect. B* **30**, 2540 (1974).
43. A. Novak. *Struct. Bonding (Berlin)* **18**, 177 (1974).
44. C. Cohen-Tannoudji, B. Diu, F. Laloë. *Mécanique Quantique*, Hermann, Paris (1977).
45. H. Sugimoto, A. Okumura, H. Yuuki. *Phys. Rev. B* **73**, 014305 (2006).
46. R. A. Cowley. *J. Phys.: Condens. Matter* **15**, 4143 (2003).
47. A. J. Leggett. *Rev. Mod. Phys.* **71**, S318 (1999).
48. S. Kashida, S. Ikeda, Y. Nakai. *J. Phys. Soc. Jpn.* **63**, 4643 (1994).
49. <http://www.isis.rl.ac.uk/excitations/mari/>.
50. S. Ikeda, S. Kashida, H. Sugimoto, Y. Yamada, S. M. Bennington, F. Fillaux. *Phys. Rev. B* **66**, 184302 (2002).
51. D. A. Keen, S. W. Lovesey. *J. Phys.: Condens. Matter* **15**, 4937 (2003).
52. D. A. Keen, S. W. Lovesey. *J. Phys.: Condens. Matter* **16**, 5637 (2004).
53. A. Zeilinger, R. Gähler, C. G. Shull, W. Treimer, W. Mampe. *Rev. Mod. Phys.* **60**, 1067 (1988).
54. S. Dürr, T. Nonn, G. Rempe. *Nature* **395**, 33 (1998).
55. A. Zeillinger. *Rev. Mod. Phys.* **71**, S288 (1999).
56. <http://www.isis.rl.ac.uk/crystallography>.
57. E. Babaev, A. Sudbø, N. W. Ashcroft. *Phys. Rev. Lett.* **95**, 105301 (2005).